Modification of Symmetry of Poloidal Eigenmode of Geodesic Acoustic Modes

Makoto SASAKI, Kimitaka ITOH[1)], Akira EJIRI[2)] and Yuichi TAKASE[2)]

Graduate School of Science, The University of Tokyo, Tokyo 113-0033, Japan
[1)]*National Institute for Fusion Science, Toki 509-5292, Japan*
[2)]*Graduate School of Frontier Sciences, The University of Tokyo, Kashiwa 277-8561, Japan*

(Received 28 April 2007 / Accepted 8 January 2008)

The poloidal eigenmode of the geodesic acoustic mode (GAM) is analyzed in the case of high aspect ratio circular plasmas, and an analytic representation for poloidal eigenfunction is derived. The $m = \pm 1$ and $m = \pm 2$ (m is the poloidal number) components of eigenfunction show up-down antisymmetry and up-down symmetry, respectively, in a torus. The mixing of the up-down symmetric and antisymmetric components becomes significant, when the ion gyroradius is large or when electron temperature is higher than ion temperature.

Keywords: zonal flow, geodesic acoustic mode, eigenmode, eigenfrequency, eigenfunction, density oscillation, collisionless damping, gyrokinetic equation

DOI: 10.1585/pfr.3.009

1. Introduction

Recently, zonal flows (ZFs) have attracted much attention in plasma research. In particular, ZFs are thought to suppress anomalous transport in toroidal plasmas, and they also play an important role in turbulent transport [1–4]. ZFs are symmetric flows on a magnetic surface (the toroidal mode number $n = 0$ and the poloidal mode number m is very close to zero), which change their sign in the radial direction and their frequency ω is nearly equal to zero. In toroidal plasmas, an oscillation symmetric mode ($n = 0, m \approx 0$) exists in addition to a static ZF. This mode arises from a nonzero divergence of the $E \times B$ drift velocity, because a magnetic field line does not correspond to a geodesic line. This oscillating mode is called a geodesic acoustic mode (GAM) [2, 5, 6] , which was found by Winsor *et al.*, using a fluid model [6]. Subsequently, a dispersion relation of the GAM was derived [7, 8]. Hinton *et al.* analyzed GAM using the gyrokinetic equation, and discussed the partition ratio of the initial impulse between GAM and ZFs [9]. GAM oscillations are associated with a small but finite $m = 1$ component, therefore they are damped by ion Landau damping. In addition to these studies, a strong collisionless damping by a finite orbit width (finite gyroradius) was studied [10, 11], and the GAM theory was extended to helical systems [10, 12, 13]. The nonlinear excitation mechanism of GAM was also studied. In Refs. [14, 15], the excitation of GAM by turbulence was confirmed using direct numerical simulation (DNS). According to a simulation, the excitation of GAM was attributed to the combination of the geometrical curvature and turbulent shear [16], based on which the condition for excitation of GAM due to microscopic turbulence was derived [17]. These studies showed that GAM was excited by turbulence in configurations with higher safety factors. In parallel with these theoretical findings, the fluctuations of density and potential of GAM were recently observed in experiments, using Heavy Ion Beam Probe and electrostatic probe, and a Doppler reflectometer [18–21]. These experimental observations require an accurate theoretical prediction of the temporal-spatial structure of the GAM eigenfunction.

The spatial structure of the GAM eigenfunction was studied based on these factors. The gyrokinetic equation and the quasi neutral condition served as the basic equations. We considered poloidal modes up to the $m = \pm 2$ components. The product of the radial wave number k of the zonal flow and the ion gyroradius ρ was assumed to be much smaller than unity. The $m = \pm 1$ and $m = \pm 2$ components have different parity in the up-down symmetry, thus influencing the symmetry property of the eigenmode. The up-down symmetric components become large when either the ion gyroradius is large or when electron temperature is higher than ion temperature.

The outline of this article is as follows. In Sec. 2, the model and basic equations are introduced, and the response function to the fluctuation in potential is derived. In Sec. 3, the eigenequation is derived, and from it the eigenvalue [11] (which represents GAM frequency and damping rate) and the eigenfunction are obtained. Further, the poloidal structure of GAM potential is derived. The results obtained were comparable to those of previous studies. A discussion and summary are provided in Sec. 4.

author's e-mail: sasaki@fusion.k.u-tokyo.ac.jp

2. Model and Basic Equation

2.1 Model

The configuration under study is assumed to be a high aspect ratio tokamak with a circular cross-section. Deviations from the circular cross-section, such as elongation and triangularity are not considered in this study. The magnetic field can be expressed as

$$\boldsymbol{B} = \frac{B_0}{1+\epsilon\cos\theta}\left(\boldsymbol{e}_\zeta + \frac{\epsilon}{q}\boldsymbol{e}_\theta\right), \tag{1}$$

where $\boldsymbol{e}_\zeta$ and $\boldsymbol{e}_\theta$ are the toroidal and poloidal directions, respectively, ϵ represents the inverse aspect ratio and q is the safety factor.

We derive a dispersion relation under the collisionless condition. The gyrokinetic equation and the quasi-neutral condition serve as the basic equations [22, 23]:

$$\left(\frac{\partial}{\partial t} + v_\parallel \boldsymbol{b}\cdot\nabla + i\boldsymbol{k}_\perp\cdot\boldsymbol{v}_{\mathrm{dr}}\right)\delta f_{k_\perp} = -\left(v_\parallel \boldsymbol{b}\cdot\nabla + i\boldsymbol{k}_\perp\cdot\boldsymbol{v}_{\mathrm{dr}}\right)\times\left(F_0 J_0(k_\perp\rho)\frac{e\phi_{k_\perp}}{T}\right), \tag{2}$$

$$\int \mathrm{d}v^3 J_0 \delta f^{(i)}_{k_\perp} - n_0\left(1-\Gamma_0(k^2\rho^2/2)\right)\frac{e\phi_{k_\perp}}{T_\mathrm{i}} = \frac{n_0}{T_\mathrm{e}}\left(\phi_{k_\perp} - \langle\phi_{k_\perp}\rangle\right). \tag{3}$$

Here, $\delta f^{(i)}_{k_\perp}$ and $\phi_{k_\perp}$ are the ion distribution function and electrostatic potential, respectively, and subscript $k_\perp$ represents the wave vector of zonal flow. The electron density fluctuation is assumed to be a Boltzmann distribution for the non-zonal component and zero for the zonal component. T_e and T_i are the electron, and ion temperatures, respectively. $\langle\cdot\rangle$ represents the magnetic surface average, F_0 is a Maxwell distribution, $J_0(x)$ is a zeroth-order Bessel function, $\Gamma_0(k^2\rho^2/2) = I_0(k^2\rho^2/2)\exp(-k^2\rho^2/2)$ (where I_0 represents a zeroth-order modefied Bessel function), ρ_i is the ion gyroradius, and $\boldsymbol{b}$ is a unit vector representing the magnetic field direction. In Eq. (2), v_{dr} represents the radial component of toroidal drift due to inhomogeneity in the toroidal field, which can be expressed as

$$v_{\mathrm{dr}} = \frac{1}{\Omega}\boldsymbol{e}_\mathrm{r}\cdot\left[\boldsymbol{b}\left(v_\parallel^2 + \frac{\mu B}{m}\right)\times\frac{\nabla B}{B}\right]. \tag{4}$$

Hereafter, we omit the subscripts in the following cases: $k_r = k$ ($k_r \gg k_\theta$), and $\delta f_{k_\perp} \to \delta f, \phi_{k_\perp} \to \phi$.

2.2 Response of the distribution function to fluctuation in potential

Assuming that the particle orbits are circular, the toroidal drift can be written as

$$k v_{\mathrm{dr}} = -\frac{v_\mathrm{T}}{qR_0}k\hat{u}\sin\theta = -s\frac{v_\mathrm{T}}{qR_0}\left(\hat{v}_\parallel^2 + \frac{\hat{v}_\perp^2}{2}\right)\sin\theta. \tag{5}$$

Here, we introduce the dimensionless variables $\hat{v_\parallel} = v_\parallel/v_\mathrm{T}$, and $\hat{v_\perp} = v_\perp/v_\mathrm{T}$. and, define the smallness parameter $s = \frac{kv_\mathrm{T}q}{\Omega}$, which represents the finite orbit width effect.

In order to derive the response of distribution function to fluctuation in potential, we transform Eq. (2) into

$$\left(\frac{\partial}{\partial t} + \frac{v_\parallel}{R_0 q}\frac{\partial}{\partial\theta}\right)\mathrm{e}^{ik\delta(\theta)}\delta f = -\frac{v_\parallel}{R_0 q}J_0(s\hat{v}_\perp/q)\frac{\partial}{\partial\theta}\left(F_0\mathrm{e}^{ik\delta(\theta)}\hat{\phi}\right) \tag{6}$$

where $\hat{\phi} = e\phi/T_\mathrm{i}$. In Eq. (6) $ik\delta(\theta)$ represents the doppler shift due to the toroidal drift motion, which can be written as

$$k\delta(\theta) = \frac{kR_0 q}{v_{\parallel 0}}\int v_{\mathrm{dr}} \approx s\left(\hat{v}_\parallel + \frac{\hat{v}_\perp^2}{2\hat{v}_\parallel}\right)\cos\theta. \tag{7}$$

Next, we perform Fourier transformation about time t and poloidal angle θ as

$$\delta f(\theta) = \sum_{m=-\infty}^{\infty}\mathrm{e}^{im\theta - i\omega t}\delta f_m(\omega), \tag{8a}$$

$$\hat{\phi}(\theta) = \sum_{m=-\infty}^{\infty}\mathrm{e}^{im\theta - i\omega t}\hat{\phi}_m(\omega). \tag{8b}$$

We then obtain the response relations between the distribution and potential for the poloidal mode number $m = 0$ from Eq. (2), and for $m \neq 0$ from Eq. (6)

$$i\hat{\omega}\delta f_0 = \frac{1}{2}J_0(s\hat{v}_\perp/q)k\hat{u}(\delta f_{-1} - \delta f_1 + \hat{\phi}_{-1} - \hat{\phi}_1), \tag{9a}$$

$$\delta f_m = \sum_{l,l'} J_0(s\hat{v}_\perp/q)F_0\frac{\hat{v_\parallel}(m-l)}{\omega - \hat{v_\parallel}(m-l)}i^{l'-l} \times J_l(k\delta_1)J_{l'}(k\delta_1)\phi_{m-l-l'}, \tag{9b}$$

where $\hat{\omega}$ is the normalized frequency defined as $\hat{\omega} = \omega R_0 q/v_\mathrm{T}$. These equations represent the response of the distribution function to the potential. The terms such as $\{\hat{v_\parallel}(m \pm l)/(\omega - \hat{v_\parallel}(m \pm l))\}i^{l'-l}J_l(k\delta_1)J_{l'}(k\delta_1)$ represent toroidal coupling with the l-th mode. Equation (9b) allows coupling with infinite terms, however the combination of higher harmonics results in a higher order of $k\rho$. Therefore, the infinite summation can be approximated by a finite summation. We only consider terms up to $m = \pm 1$ in the determination of the real frequency.

In addition to this truncation, the GAM possesses the following symmetries

$$\delta f_m(v_\parallel) = (-1)^m \delta f_{-m}(-v_\parallel), \tag{10a}$$

$$\phi_m = (-1)^m \phi_{-m}, \tag{10b}$$

which allow simplification in calculation. In particular, δf_2, and $\delta f_1, \delta f_0$ can be written explicitly as

$$i\hat{\omega}\delta f_0 = C_{00}\phi_0 + C_{01}\phi_1 + C_{02}\phi_2, \tag{11a}$$

$$\delta f_1 = C_{10}\phi_0 + C_{11}\phi_1 + C_{12}\phi_2, \tag{11b}$$

$$\delta f_2 = C_{20}\phi_0 + C_{21}\phi_1 + C_{22}\phi_2. \tag{11c}$$

The coefficients C_{ij} are discussed in Appendix A. Integrating Eq. (11a-c) in the whole velocity space, and using

Eq. (3), which is a quasi-neutrality condition, we obtain the following equations:

$$in_0\hat{\omega}\frac{s^2}{2q^2}\hat{\phi}_0 = \int C_{00}d^3v\hat{\phi}_0 + \int C_{01}d^3v\hat{\phi}_1 + \int C_{02}d^3v\hat{\phi}_2, \tag{12a}$$

$$n_0\frac{1}{\tau_e}\phi_1 = \int C_{10}d^3v\hat{\phi}_0 + \int C_{11}d^3v\hat{\phi}_1 + \int C_{22}d^3v\hat{\phi}_2, \tag{12b}$$

$$n_0\frac{1}{\tau_e}\phi_1 = \int C_{20}d^3v\hat{\phi}_0 + \int C_{21}d^3v\hat{\phi}_1 + \int C_{22}d^3v\hat{\phi}_2. \tag{12c}$$

3. Eigenvalue and Eigenfunction

3.1 Eigenequation

In this section, we derive the explicit form of the eigenequation. Equations (12a-c) can be expressed in matrix form as follows:

$$\begin{pmatrix} D_{00} & D_{01} & D_{02} \\ D_{10} & D_{11} & D_{12} \\ D_{20} & D_{21} & D_{22} \end{pmatrix}\begin{pmatrix} \hat{\phi}_0 \\ \hat{\phi}_1 \\ \hat{\phi}_2 \end{pmatrix} = 0. \tag{13}$$

The coefficients in Eq. (13) can be derived as

$$D_{00} = i\hat{\omega}\frac{s^2}{2q^2}n_0 + n_0 i\frac{s^2}{2}\left[\frac{1}{2}\hat{\omega} + \hat{\omega}^3 + \hat{\omega}^4 Z(\hat{\omega}) + \hat{\omega}\left(1+\hat{\omega}Z(\hat{\omega})\right)\right.$$
$$\left. + i\sqrt{\pi}\frac{s^2}{8}\left(\frac{6}{\hat{\omega}^2} + 3 + \frac{3}{4}\hat{\omega}^2 + \frac{\hat{\omega}^4}{16} + \frac{\hat{\omega}^6}{64}\right)e^{-\hat{\omega}^2/4}\right], \tag{14a}$$

$$D_{01} = n_0 s\left[\hat{\omega}^2 + \left(\frac{1}{2}\hat{\omega} + \hat{\omega}^3\right)Z(\hat{\omega})\right.$$
$$\left. + i\sqrt{\pi}\frac{s^2}{4}\left(\frac{3}{2\hat{\omega}} + \frac{3}{4}\hat{\omega} + \frac{3}{16}\hat{\omega}^3 + \frac{\hat{\omega}^5}{32}\right)e^{-\hat{\omega}^2/4}\right], \tag{14b}$$

$$D_{02} = i\frac{1}{2}ns^2\left[\frac{3}{4}\hat{\omega} + \frac{7}{8}\hat{\omega}^3 + \left(\frac{1}{2} + \hat{\omega}^2 + \hat{\omega}^4\right)Z(\hat{\omega})\right.$$
$$\left. - i\sqrt{\pi}\left(\frac{1}{2} + \frac{\hat{\omega}^2}{4} + \frac{\hat{\omega}^4}{16}\right)e^{-\hat{\omega}^2/4}\right], \tag{14c}$$

$$D_{10} = i\frac{n_0 s}{2}\left[\hat{\omega} + \left(\hat{\omega}^2 + \frac{1}{2}\right)Z(\hat{\omega})\right.$$
$$\left. + i\sqrt{\pi}\frac{s^2}{8}\left(\frac{3}{\hat{\omega}^2} + \frac{3}{2}\frac{3}{8}\hat{\omega}^2 + \frac{\hat{\omega}^4}{16}\right)e^{-\hat{\omega}^2/4}\right], \tag{14d}$$

$$D_{11} = n_0\frac{1}{\tau_e} + n_0\left[1 + \hat{\omega}Z(\hat{\omega})\right.$$
$$\left. + i\sqrt{\pi}s^2\left(\frac{1}{\hat{\omega}} + \frac{\hat{\omega}}{2} + \frac{\hat{\omega}^3}{8}\right)e^{-\hat{\omega}^2/4}\right], \tag{14e}$$

$$D_{12} = i\frac{1}{2}n_0 s\left[-\frac{\hat{\omega}}{2} - \left(\frac{1}{2} + \hat{\omega}^2\right)Z(\hat{\omega}) + i\sqrt{\pi}\left(\frac{1}{2} + \frac{\hat{\omega}^2}{4}\right)e^{-\hat{\omega}^2/4}\right], \tag{14f}$$

$$D_{20} = -\frac{1}{8}n_0 s^2\left[\frac{3}{2} + \frac{\hat{\omega}^2}{4} + i\sqrt{\pi}\left(\frac{1}{\hat{\omega}} + \frac{\hat{\omega}}{2} + \frac{\hat{\omega}^3}{8}\right)e^{-\hat{\omega}^2/4}\right], \tag{14g}$$

$$D_{21} = i\frac{1}{2}n_0 s\left\{-\frac{\hat{\omega}}{2} - \left(\frac{1}{2} + \hat{\omega}^2\right)Z(\hat{\omega})\right.$$
$$\left. + i\sqrt{\pi}\left(\frac{1}{2} + \frac{\hat{\omega}^2}{4}\right)e^{-\hat{\omega}^2/4}\right\}, \tag{14h}$$

$$D_{22} = n_0\frac{1}{\tau_e} + n_0 i\sqrt{\pi}\left(1 + \frac{\hat{\omega}}{2}\right)e^{-\hat{\omega}^2/4}. \tag{14i}$$

In order to clarify the s-ordering, we introduce d_{ij}, and e_{ij} as

$$D_{0j} = n_0 s^2\left(d_{0j} + s^2 e_{0j}\right), \tag{15a}$$

$$D_{j0} = n_0 s^2\left(d_{j0} + s^2 e_{j0}\right) \quad (j = 0, 2), \tag{15b}$$

$$D_{ii} = n_0\left(d_{j0} + s^2 e_{j0}\right) \quad (i = 1, 2), \tag{15c}$$

$$D_{ij} = n_0 s\left(d_{ij} + s^2 e_{ij}\right) \quad \text{(others)}. \tag{15d}$$

Next, we derive the dispersion relation, which is the determinant of D_{ij}. We include only the real parts of terms up to $O(s^2)$ and the imaginary parts of terms up to $O(s^4)$. The dispersion relation can be written as

$$\Delta = s^2\left\{\Delta_r + i\left(\Delta_{i0} + s^2\Delta_{i1}\right)\right\} = 0, \tag{16}$$

where Δ_r determines the real frequency of GAM, Δ_{i0} represents the fundamental property of GAM in terms of an imaginary frequency, and Δ_{i1} represents the finite ion gyroradius effect in terms of an imaginary frequency of the s^2-order. These terms are written as

$$\Delta_{r0} = Re\begin{vmatrix} d_{00} & d_{01} \\ d_{10} & d_{11} \end{vmatrix}, \tag{17a}$$

$$\Delta_{i0} = Im\begin{vmatrix} d_{00} & d_{01} \\ d_{10} & d_{11} \end{vmatrix}, \tag{17b}$$

$$\Delta_{i1} = Im\left[\begin{vmatrix} e_{00} & e_{01} \\ d_{10} & d_{11} \end{vmatrix} + \begin{vmatrix} d_{00} & d_{01} \\ e_{10} & e_{11} \end{vmatrix}\right.$$
$$\left. + \left\{-\frac{d_{12}}{d_{22}}\begin{vmatrix} d_{00} & d_{01} \\ d_{20} & d_{21} \end{vmatrix} + \frac{d_{02}}{d_{22}}\begin{vmatrix} d_{10} & d_{11} \\ d_{20} & d_{21} \end{vmatrix}\right\}\right]. \tag{17c}$$

3.2 Eigenvalue

Here, we derive the fundamental eigenvalue by solving the fundamental dispersion relation

$$\Delta_{r0} + i\left(\Delta_{i0} + s^2\Delta_{i1}\right) = 0. \tag{18}$$

Since, we are considering the GAM frequency, we apply the $\hat{\omega} \gg 1$ approximation, and expand the plasma dispersion function asymptotically. The expanded coefficients d_{ij}, and e_{ij} are discussed in the appendix. The real frequency is determined by substituting $\Delta_{r0} = 0$, and the imaginary part is assumed to be much smaller than the real part, i.e., $\hat{\omega} \gg \hat{\gamma}$. The fundamental dispersion relation is approximated up to $O(\hat{\gamma})$, where $\hat{\gamma}$ can be obtained as

$$\Delta_{r0}(\hat{\omega} + \hat{\gamma}) + i\left(\Delta_{i0}(\hat{\omega} + \hat{\gamma}) + s^2\Delta_{i1}(\hat{\omega} + \hat{\gamma})\right)$$
$$\approx \Delta_{r0}(\hat{\omega}) + i\left(\frac{\partial\Delta_{r0}(\hat{\omega}_0)}{\partial\hat{\omega}}\hat{\gamma} + \Delta_0(\hat{\omega}) + s^2\Delta_{i1}(\hat{\omega})\right) = 0 \tag{19}$$

$$\leftrightarrow \hat{\gamma} \approx -\frac{\Delta_{i0} + s^2\Delta_{i1}}{\partial\Delta_{r0}/\partial\hat{\omega}}. \tag{20}$$

Thus, the lowest order estimate for ω can be derived as

$$\omega_0 = \omega_{\rm G}^{(0)} + i\gamma_{\rm G}^{(0)}, \tag{21}$$

$$\omega_{\rm G}^{(0)} = \sqrt{\frac{7}{4} + \tau_{\rm e}}\frac{v_{\rm T}}{R_0}\left[1 + 2\frac{23 + 16\tau_{\rm e} + 4\tau_{\rm e}^2}{(7 + 4\tau_{\rm e})^2 q^2}\right]^{1/2}, \tag{22}$$

$$\begin{aligned}\gamma_{\rm G}^{(0)} = &- \sqrt{\pi}q\tau_{\rm e}\frac{v_{\rm T}}{2R_0}\left[1 + 2\frac{23 + 16\tau_{\rm e} + 4\tau_{\rm e}^2}{(7 + 4\tau_{\rm e})^2 q^2}\right]^{-1}\\ &\times\left\{\left(\hat{\omega}_{\rm G}{}^4\frac{1}{\tau_{\rm e}} + \hat{\omega}_{\rm G}{}^2\frac{1}{\tau_{\rm e}} + \frac{3}{2}\hat{\omega}_{\rm G}{}^2\right)\mathrm{e}^{-\hat{\omega}_{\rm G}{}^2}\right.\\ &+ \frac{1}{8}s^2\mathrm{e}^{-\hat{\omega}_{\rm G}{}^2/4}\left(\frac{1}{64\tau_{\rm e}}\hat{\omega}_{\rm G}{}^6 + \left(\frac{15}{128}\right.\right.\\ &\left.\left.\left.+ \frac{1}{8\tau_{\rm e}} + \frac{1}{4q^2}\right)\hat{\omega}_{\rm G}{}^4 + \left(\frac{3}{4\tau_{\rm e}} + \frac{93}{256}\right)\hat{\omega}_{\rm G}{}^2\right)\right\}. \end{aligned}\tag{23}$$

In the above equations, the terms containing $\exp\left(-\hat{\omega}_{\rm G}^2/4\right)$ represent the Landau damping effect as pointed out by Sugama and Watanabe [11, 12]. The coefficient of $\exp\left(-\hat{\omega}_{\rm G}^2/4\right)$ in Eq. (23) has been modified, and the leading term is expressed as $1/8 \times 1/64\tau_{\rm e}$.

3.3 Eigenfunction

3.3.1 potential eigenfuction

The poloidal eigenfunction can be derived from the eigen equation Eq. (13). Here, we transform Eq. (13) into

$$\begin{pmatrix} D_{11} & D_{12} \\ D_{21} & D_{22} \end{pmatrix}\begin{pmatrix} \phi_1/\phi_0 \\ \phi_2/\phi_0 \end{pmatrix} = -\begin{pmatrix} D_{10} \\ D_{20} \end{pmatrix}. \tag{24}$$

From this equation, we can obtain

$$\frac{\phi_1}{\phi_0} = \frac{D_{12}D_{20} - D_{22}D_{10}}{D_{11}D_{22} - D_{12}D_{21}} \approx i\frac{1}{2}\frac{s\tau_{\rm e}}{\hat{\omega}}, \tag{25a}$$

$$\frac{\phi_2}{\phi_0} = \frac{D_{21}D_{10} - D_{11}D_{20}}{D_{11}D_{22} - D_{12}D_{21}} \approx -\frac{s^2\tau_{\rm e}}{\hat{\omega}^2}\left(\frac{1}{4}\tau_{\rm e} + \frac{7}{8}\right). \tag{25b}$$

Considering the parity of Fourier components ($\phi_{-m} = (-1)^m\phi_m$), the poloidal eigenfunction can be expressed as

$$\begin{aligned}\frac{\phi(\theta)}{\phi_0} &= \sum_m \mathrm{e}^{im\theta}\phi_m\\ &\approx 1 - \frac{s\tau_{\rm e}}{\hat{\omega}_{\rm G}}\sin\theta - \frac{s^2\tau_{\rm e}}{\hat{\omega}_{\rm G}{}^2}\left(\frac{1}{2}\tau_{\rm e} + \frac{7}{4}\right)\cos 2\theta.\end{aligned} \tag{26}$$

The value of the GAM potential is nearly constant on the magnetic surface, and dependence on θ is introduced by a small but finite ion-gyroradius effect.

The signs of k and u are important when analyzing the spatial structure of the eigenfunction. The general wave (composed of traveling and the standing waves), can be expressed by the superimposing waves that are propagating toward $r > 0$ and $r < 0$. For $\omega > 0$, we need to consider both positive and negative values of k. In this paper, positive ω is chosen as a convention. Here, the waves of $k > 0$ and $k < 0$ represent traveling waves propagating toward $r > 0$ and $r < 0$, respectively. When the amplitudes of these components are the same, resulting wave represents a standing wave.

propagating wave First, we discuss the case of the unidirectional radially propagating wave. Here we consider $k > 0$. In this case, the spatial structure of the eigenfunction can be written as

$$\begin{aligned}\frac{\phi(r,\theta)}{\phi_0} \approx &\left\{1 - \frac{s\tau_{\rm e}}{\hat{\omega}_{\rm G}}\sin\theta - \frac{s^2\tau_{\rm e}}{\hat{\omega}_{\rm G}{}^2}\left(\frac{1}{2}\tau_{\rm e} + \frac{7}{4}\right)\cos 2\theta\right\}\\ &\times\cos(kr - \omega_{\rm G}t).\end{aligned} \tag{27}$$

As seen in Eq. (27), the structure determined by Eq. (26) propagates radially. The $m = \pm 1$ components has a $\sin\theta$ dependency, which shows an up-down antisymmetry against the midplane of the torus. Its amplitude $k\rho q\tau_{\rm e}/\hat{\omega}_{\rm G}$ depends on the sign of the phase of electric field k (when the direction of increase in $E \times B$ drift velocity is positive along the z-axis, the eigen function increases along the positive z-axis). The $m = \pm 2$ components have a $\cos 2\theta$ dependence, which has an up-down symmetry in the torus. Its amplitude is approximately $\sim k^2\rho^2 q^2\tau_{\rm e}^2/\hat{\omega}_{\rm G}^2$, which is independent of the sign of k. This component becomes larger when the ion gyroradius is large or when the electron temperature is higher than the ion temperature; it is almost independent of q because the leading term of $\hat{\omega}_{\rm G}$ is proportional to q. In addition, the $m = \pm 2$ components always reduce the amplitude of the $m = 0$ component at $\theta = 0, \pi$ and they intensify at $\theta = \pm\pi/2$. The amplitude of $m = \pm 1$ is intensified positively in the bottom of the torus ($\theta = 3\pi/2$) by the $m = \pm 2$ components. The region satisfying the condition of $|\phi(\theta)| < |\phi_0|$ widens. As seen in Eq. (26), the $m = \pm 1$ component can be deduced from the values of $\phi(\theta)$ at $\theta = \pi/4$. Once the $m = \pm 1$ component is determined, the $m = \pm 2$ component can be deduced by comparing the $\phi(\theta)$ values at $\theta = 0, \pi/2$.

standing wave We now discuss the case of the standing wave. The lowest order term, i.e. the $m = 0$ component, can be written as

$$\begin{aligned}\Big\{\phi(r,\theta)\Big\}_{m=0} = \phi_0\Big\{&\exp i\,(kr - \omega_{\rm G}t)\\ &+ \exp i\,(-kr - \omega_{\rm G}t - i\delta)\Big\}.\end{aligned} \tag{28}$$

In this case, the spatial structure of the eigenfunction can be written as

$$\begin{aligned}\frac{\phi(r,\theta)}{\phi_0} \approx \Bigg[&\left\{2 - 2\frac{s^2\tau_{\rm e}}{\hat{\omega}_{\rm G}{}^2}\left(\frac{1}{2}\tau_{\rm e} + \frac{7}{4}\right)\cos 2\theta\right\}\\ &\times\cos k\left(r - \frac{\delta}{2k}\right)\cos\omega_{\rm G}\left(t - \frac{\delta}{2\omega_{\rm G}}\right)\\ &+ 2\frac{s\tau_{\rm e}}{\hat{\omega}_{\rm G}}\sin\theta\sin k\left(r - \frac{\delta}{2k}\right)\\ &\times\sin\omega_{\rm G}\left(t - \frac{\delta}{2\omega_{\rm G}}\right)\Bigg].\end{aligned} \tag{29}$$

Here, δ denotes the phase difference between the waves with $k > 0$ and $k < 0$. This phase difference is not essential, because we can eliminate it by shifting the origin of time and space. Unlike the case of the propagating wave, the structure does not propagate radially, but oscillates temporally. As Eq. (29) shows, the time and radial dependences of $m = \pm 1$ and $m = \pm 2$ components differ from each other. Therefore, the poloidal angle that satisfies $\phi(\theta) = \phi_0$ at a certain radius changes with time. Furthermore, at a certain time ($t = \delta/2\omega_G + n\pi, n = 0, 1, 2 \ldots$), the $m = \pm 1$ components disappear, whereas the $m = 0, \pm 2$ components remain. In contrast, at time $t = \delta/2\omega_G + (n + 1/2)\pi$, the $m = 0, \pm 2$ components disappear, and only the $m = \pm 1$ components remain. The structure has a radial periodicity of $2\pi/k$ when the time is fixed, and has a time periodicity of $2\pi/\omega_G$ when the radial position is fixed. Furthermore, in the case of the general wave, which can be expressed by superimposing the propagating and the standing waves, the effect of the $m = \pm 2$ components on the $m = \pm 1$ components vary radially.

3.3.2 density eigenfuction

Because the density eigenfunction is more easily observed, we explain the density fluctuation. The electron density fluctuation is obtained from Eq. (3), and is expressed as

$$\frac{\tilde{n}(\theta)}{n_0} = \hat{\phi}_0 \left\{ -\frac{s\tau_e}{\hat{\omega_G}} \sin\theta - \frac{s^2\tau_e}{\hat{\omega_G}^2} \left(\frac{1}{2}\tau_e + \frac{7}{4} \right) \cos 2\theta \right\}. \tag{30}$$

Radially propagating and standing waves are reconstructed by choosing an appropriate sign for k.

propagating wave First, we discuss the case of the unidirectional radially propagating wave. Here we select k as $k > 0$. In this case, the density structure of the eigenfunction can be written as

$$\frac{\tilde{n}(r,\theta)}{n_0} = \hat{\phi}_0 \left\{ -\frac{s\tau_e}{\hat{\omega_G}} \sin\theta - \frac{s^2\tau_e}{\hat{\omega_G}^2} \left(\frac{1}{2}\tau_e + \frac{7}{4} \right) \cos 2\theta \right\} \times \cos(kr - \omega_G t). \tag{31}$$

It is found that the θ dependent structure propagates radially. The leading order of the density fluctuation is approximately $k\rho$, and shows $\sin\theta$ dependence, which is antisymmetric in the torus. Similar to the potential eigenfunction, the $m = \pm 1$ components depend on the sign of k, whereas the $m = \pm 2$ components are independent of it. The behavior of density eigenfunction is shown in Fig. 1 for a fixed the time and radial position ($kr - \omega_G t = 2n\pi, n = 0, 1, 2 \ldots$). Although the sign of the density eigenfunction changes in the vertical direction, the up-down antisymmetry is broken.

To show the effect of breaking of antisymmetry, we analyze the ratio between the top and bottom, (i.e., $\tilde{n}(3\pi/2)$ and $\tilde{n}(\pi/2)$, in Fig. 2), which is always unity when antisymmetry holds. It is found that $\tilde{n}(3\pi/2)/\tilde{n}(3\pi/2)$ increases when $k\rho$ becomes large, which indicates that the antisymmetry increases. When $k\rho \sim 0.1$, this antisymmetry is several tens of percent of the density fluctuation, which can be observed. In addition, we analyze the poloidal angles which the density fluctuation becomes zero at all times (these points are defined as θ_0, and θ_1). When $k\rho$ is small, the density fluctuation is nearly antisymmetric, resulting in zero points of $\theta_0 = 0$, and $\theta_1 = \pi$. However, if $k\rho$ becomes larger, the antisymmetry breaks down, therefore θ_0, and θ_1 moves from 0, π to $0 - \Delta\theta$, $\pi + \Delta\theta$, respectively. The behavior of $\Delta\theta$ is shown in Fig. 3, in which it is possible to detect the density fluctuation at the midplane. The density perturbations for the (r, θ) plane are illustrated in Fig. 4. The boundary for $\tilde{n}/n = 0$ shifts from $\theta = 0, \pi$ as seen in Fig. 3. This pattern propagates in the r-direction.

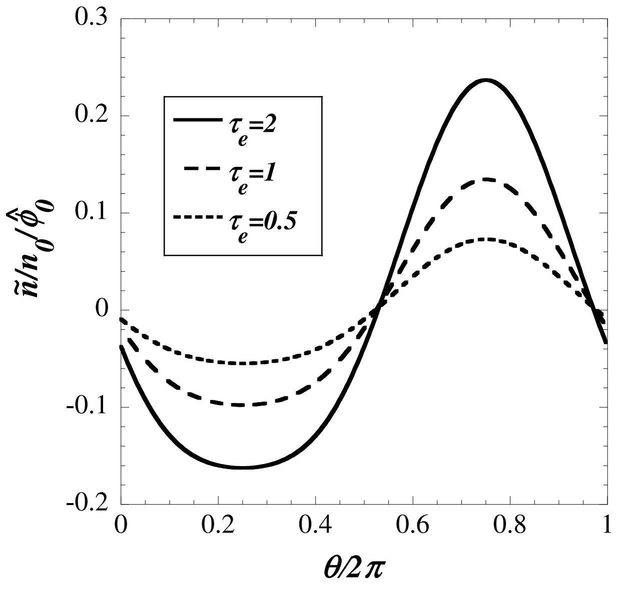

Fig. 1 Eigenfunctions for several τ_e ($\tau_e = 0.5, 1, 2$), with $k\rho = 0.1$, and $q = 3$.

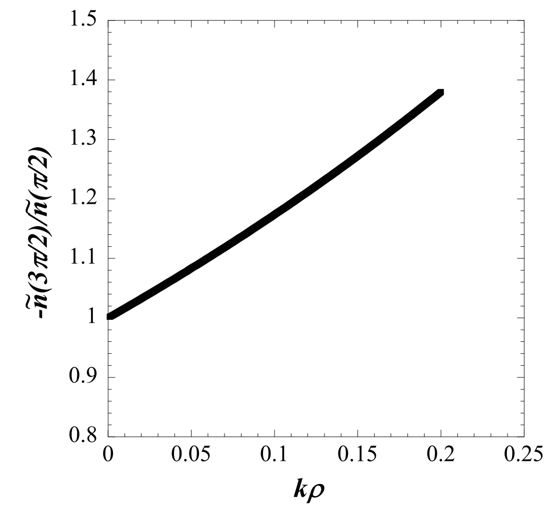

Fig. 2 $k\rho$ dependence of the asymmetry in density perturbation. Asymmetry is defined as $\tilde{n}(3\pi/2)/\tilde{n}(\pi/2)$, for $q = 3$, and $\tau_e = 1$.

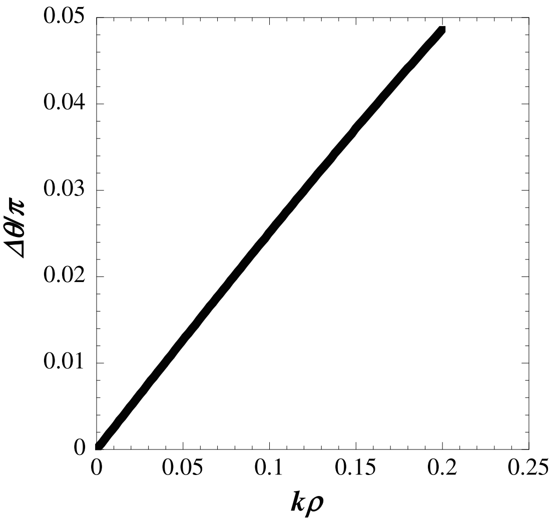

Fig. 3 $k\rho$ dependence of the points where the density fluctuation becomes zero, for $q = 3$, and $\tau_e = 1$.

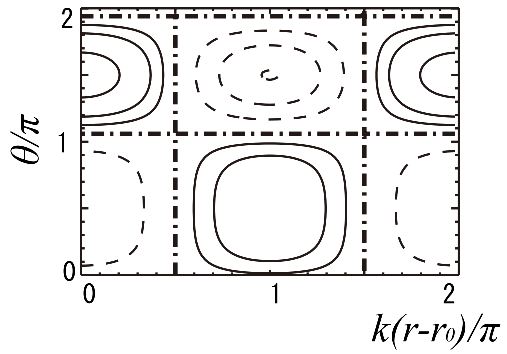

Fig. 4 Spatial structure of density fluctuation in propagating wave on the (r, θ) plane at $\omega_G(t - t_0) = 2n\pi$, n is an integer, and $t_0 = \delta/2k$. The solid line shows the contour of $\tilde{n}/n\phi_0 > 0$, the dashed line shows the contour of $\tilde{n}/n\phi_0 < 0$, and the dash-dot line shows the contours of $\tilde{n}/n\phi_0 = 0$.

standing wave Next, we discuss the case of the standing wave based on Eq. (28). Here, the spatial structure of the density eigenfunction can be written as

$$\frac{\tilde{n}(r,\theta)}{n_0} = \hat{\phi}_0 \left\{ 2\frac{s\tau_e}{\hat{\omega_G}} \sin\theta \sin k\left(r - \frac{\delta}{2k}\right) \times \sin\omega_G\left(t - \frac{\delta}{2\omega_G}\right) - 2\frac{s^2\tau_e}{\hat{\omega_G}^2}\left(\frac{1}{2}\tau_e + \frac{7}{4}\right) \times \cos 2\theta \cos k\left(r - \frac{\delta}{2k}\right) \cos\omega_G\left(t - \frac{\delta}{2\omega_G}\right)\right\}. \tag{32}$$

As seen in this equation, the effect of the $m = \pm 2$ components on $m = \pm 1$ components changes radially, similar to the potential eigenfunction. Unlike the case of the propagating wave, the region of $\tilde{n}/n\hat{\phi}_0 < 0$ changes both radially and temporally, which is shown in Fig. 5. The time origin is defined as the time when the $m = \pm 1$ components disappear, $t = \delta/2\omega_G + 2n\pi$. This variation in the pattern of the standing wave is compared to that of the propagating wave shown in Fig. 4. The θ-dependent structure moves in the r-direction without changing its shape in the case of the propagating wave, whereas the pattern itself changes in the case of the standing wave.

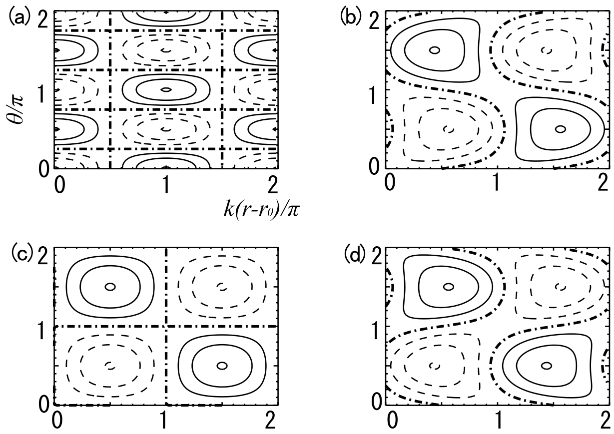

Fig. 5 Spatial structures of the density fluctuation in the standing wave on the (r, θ) plane. (a) at $\omega_G(t - t_0) = 2n\pi$, (b) at $\omega_G(t - t_0) = \pi/4 + 2n\pi$, (c) at $\omega_G(t - t_0) = \pi/2 + 2n\pi$, and (d) at $\omega_G(t - t_0) = 3\pi/4 + 2n\pi$. The solid line shows the contour of $\tilde{n}/n\phi_0 > 0$, the dashed line shows the contour of $\tilde{n}/n\phi_0 < 0$, and the dash-dot line shows the contours of $\tilde{n}/n\phi_0 = 0$.

Finally, we comment on the phase difference between $\tilde{n}$ and ϕ, where we consider only the dominant terms for simplicity (i.e. the $m = 0$ component in ϕ and the $m = \pm 1$ components in $\tilde{n}$). It is observed that propagating waves have peaks at the same radial location ($kr - \omega_G t = 2n\pi$), whereas standing waves have peaks that shift radially by $k\Delta r = \pi/2$.

4. Summary

In this study, the spatial structure of the GAM poloidal eigenfunction was analzsed. The analytical representations of the potential and density eigenfunctions were obtained. The eigenfunction of the $m = \pm 1$ components showed the up-down antisymmetry in the torus, and the $m = \pm 2$ components showed up-down symmetry in the torus. The mixing of the up-down symmetric and antisymmetric components becomes significant, when the ion gyroradius is large or when the electron temperature is higher than the ion temperature. The asymmetry defined by $-\tilde{n}(3\pi/2)/\tilde{n}(\pi/2)$ is approximately several tens of percent of density fluctuation, which can be observed. Cases for both propagating and standing waves are illustrated. These results will be useful in future experimental studies of GAM in toroidal plasmas.

5. Acknowledgement

The authors thank Prof. H. Sugama and the reviewer of this paper for useful discussions. This work was partly supported by a Grant-in-Aid for Scientific Research (193604918), by a Grant-in-Aid for Specially-Promoted Research (16002005), by the Collaboration Program of NIFS (NIFS06KDAD005), and by the University of Tokyo 21st Century COE Program (200300G2).

Appendix A. Coefficients (C_{ij})

The coefficients of the response of ion distribution to fluctuation in potential, from Eq. (11c), are obtained as

$$C_{00} = -\frac{1}{2}k\hat{u}F_0\left\{\frac{1}{2}i(k\delta)\left(\frac{\hat{v}_\parallel}{\hat{\omega}-\hat{v}_\parallel}+\frac{\hat{v}_\parallel}{\hat{\omega}+\hat{v}_\parallel}\right) + \frac{1}{16}i(k\delta)^3\left(\frac{2\hat{v}_\parallel}{\hat{\omega}-2\hat{v}_\parallel}+\frac{2\hat{v}_\parallel}{\hat{\omega}+2\hat{v}_\parallel}\right)\right\}, \tag{A.1}$$

$$C_{01} = -\frac{1}{2}k\hat{u}F_0\left\{\frac{\hat{v}_\parallel}{\hat{\omega}-\hat{v}_\parallel}-\frac{\hat{v}_\parallel}{\hat{\omega}+\hat{v}_\parallel}+2 + \frac{1}{4}(k\delta)^2\left(\frac{2\hat{v}_\parallel}{\hat{\omega}-2\hat{v}_\parallel}-\frac{2\hat{v}_\parallel}{\hat{\omega}+2\hat{v}_\parallel}\right)\right\}, \tag{A.2}$$

$$C_{02} = -\frac{1}{2}k\hat{u}F_0\left\{-\frac{1}{2}i(k\delta)\left(\frac{2\hat{v}_\parallel}{\hat{\omega}-2\hat{v}_\parallel}+\frac{2\hat{v}_\parallel}{\hat{\omega}+2\hat{v}_\parallel} - \frac{\hat{v}_\parallel}{\hat{\omega}-\hat{v}_\parallel}-\frac{\hat{v}_\parallel}{\hat{\omega}+\hat{v}_\parallel}\right) + \frac{1}{16}i(k\delta)^3\left(\frac{3\hat{v}_\parallel}{\hat{\omega}-3\hat{v}_\parallel}+\frac{3\hat{v}_\parallel}{\hat{\omega}+3\hat{v}_\parallel}\right)\right\}, \tag{A.3}$$

$$C_{10} = F_0\left\{i\frac{1}{2}(k\delta)\frac{\hat{v}_\parallel}{\hat{\omega}-\hat{v}_\parallel}+i\frac{1}{16}(k\delta)^3\frac{2\hat{v}_\parallel}{\hat{\omega}-2\hat{v}_\parallel}\right\}, \tag{A.4}$$

$$C_{11} = F_0\left\{\frac{\hat{v}_\parallel}{\hat{\omega}-\hat{v}_\parallel}+\frac{1}{4}(k\delta)^2\frac{2\hat{v}_\parallel}{\hat{\omega}-2\hat{v}_\parallel}\right\}, \tag{A.5}$$

$$C_{12} = F_0\left\{i\frac{1}{2}(k\delta)\left(\frac{\hat{v}_\parallel}{\hat{\omega}-\hat{v}_\parallel}-\frac{2\hat{v}_\parallel}{\hat{\omega}-2\hat{v}_\parallel}\right) - i\frac{1}{16}(k\delta)^3\frac{3\hat{v}_\parallel}{\hat{\omega}-3\hat{v}_\parallel}\right\}, \tag{A.6}$$

$$C_{20} = F_0\left\{-\frac{1}{8}(k\delta)^2\frac{2\hat{v}_\parallel}{\hat{\omega}-2\hat{v}_\parallel} + (k\delta)^4\left(\frac{1}{32}\frac{2\hat{v}_\parallel}{\hat{\omega}-2\hat{v}_\parallel}-\frac{1}{96}\frac{3\hat{v}_\parallel}{\hat{\omega}-3\hat{v}_\parallel}\right)\right\}, \tag{A.7}$$

$$C_{21} = F_0\left\{i\frac{1}{2}(k\delta)\left(\frac{2\hat{v}_\parallel}{\hat{\omega}-2\hat{v}_\parallel}-\frac{\hat{v}_\parallel}{\hat{\omega}-2\hat{v}_\parallel}\right) + i(k\delta)^3\left(\frac{1}{16}\frac{3\hat{v}_\parallel}{\hat{\omega}-3\hat{v}_\parallel}-\frac{1}{6}\frac{2\hat{v}_\parallel}{\hat{\omega}-2\hat{v}_\parallel}\right)\right\}, \tag{A.8}$$

$$C_{22} = F_0\left\{\frac{2\hat{v}_\parallel}{\hat{\omega}-2\hat{v}_\parallel} + (k\delta)^2\left(-\frac{1}{2}\frac{2\hat{v}_\parallel}{\hat{\omega}-2\hat{v}_\parallel}+\frac{1}{4}\frac{3\hat{v}_\parallel}{\hat{\omega}-3\hat{v}_\parallel}\right)\right\}. \tag{A.9}$$

Appendix B. Expansion of d_{ij}, and e_{ij}

d_{ij} and e_{ij} defined in Eqs. (15a)-(15d) are coefficients of the response of density fluctuation to fluctuation in potential. These coefficients have $Z(\hat{\omega})$ terms. In the case of GAM, since $\hat{\omega} \gg 1$ is satisfied, it is possible to expand $Z(\hat{\omega})$. From this expansion, d_{ij} and e_{ij} can be written as

$$d_{00} \approx i\hat{\omega}\frac{1}{2q^2} - i\frac{1}{2}\left(\frac{7}{4}\frac{1}{\hat{\omega}}+\frac{23}{8}\frac{1}{\hat{\omega}^3}\right) + i\frac{1}{2}i\sqrt{\pi}\left(\hat{\omega}^4+\hat{\omega}^2+\frac{1}{2}\right)\mathrm{e}^{-\hat{\omega}^2}, \tag{B.1}$$

$$d_{01} \approx -\left(1+\frac{1}{\hat{\omega}^2}+\frac{1}{\hat{\omega}^4}\right)+i\sqrt{\pi}\frac{1}{2}\hat{\omega}\mathrm{e}^{-\hat{\omega}^2}, \tag{B.2}$$

$$d_{02} \approx i\frac{1}{2}\left\{\frac{7}{4}\frac{1}{\hat{\omega}}+\frac{161}{8}\frac{1}{\hat{\omega}^3} - i\sqrt{\pi}\mathrm{e}^{-\hat{\omega}^2/4}\left(\frac{1}{2}+\frac{1}{4}\hat{\omega}^2+\frac{1}{16}\hat{\omega}^4\right)\right\}, \tag{B.3}$$

$$d_{10} \approx i\frac{1}{2}\left\{-\left(\frac{1}{\hat{\omega}}+\frac{1}{\hat{\omega}^3}\right)+i\sqrt{\pi}\left(\hat{\omega}^2+\frac{1}{2}\right)\right\}, \tag{B.4}$$

$$d_{11} \approx \frac{1}{\tau_\mathrm{e}}-\left(\frac{1}{2}\frac{1}{\hat{\omega}^2}+\frac{3}{4}\frac{1}{\hat{\omega}^4}\right)+i\sqrt{\pi}\hat{\omega}\mathrm{e}^{-\hat{\omega}^2}, \tag{B.5}$$

$$d_{12} \approx i\frac{1}{2}\left\{-\frac{1}{\hat{\omega}}-\frac{7}{\hat{\omega}^3}+i\sqrt{\pi}\left(\frac{1}{4}\hat{\omega}^2+\frac{1}{2}\right)\mathrm{e}^{-\hat{\omega}^2/4}\right\}, \tag{B.6}$$

$$d_{20} \approx -\frac{1}{8}\left\{-\frac{7}{\hat{\omega}^2}-\frac{46}{\hat{\omega}^4}+i\sqrt{\pi}\mathrm{e}^{-\hat{\omega}^2/4}\left(\frac{1}{\hat{\omega}}+\frac{\hat{\omega}}{2}+\frac{\hat{\omega}^3}{8}\right)\right\}, \tag{B.7}$$

$$d_{21} \approx i\frac{1}{2}\left\{-\frac{1}{\hat{\omega}}-\frac{7}{\hat{\omega}^3}+i\sqrt{\pi}\mathrm{e}^{-\hat{\omega}^2/4}\left(\frac{1}{4}\hat{\omega}^2+\frac{1}{2}\right)\right\}, \tag{B.8}$$

$$d_{22} \approx \frac{1}{\tau_\mathrm{e}}-\frac{2}{\hat{\omega}^2}-\frac{12}{\hat{\omega}^4}+i\sqrt{\pi}\frac{\hat{\omega}}{2}\mathrm{e}^{-\hat{\omega}^2/4}, \tag{B.9}$$

$$e_{00} \approx i\frac{1}{2}\left\{i\sqrt{\pi}\frac{1}{8}\mathrm{e}^{-\hat{\omega}^2/4}\left(\frac{6}{\hat{\omega}^2}+3+\frac{3}{4}\hat{\omega}^2+\frac{\hat{\omega}^4}{16}+\frac{\hat{\omega}^6}{64}\right)\right\}, \tag{B.10}$$

$$e_{01} \approx \frac{1}{4}i\sqrt{\pi}\mathrm{e}^{-\hat{\omega}^2/4}\left(\frac{3}{2}\frac{1}{\hat{\omega}}+\frac{3}{4}\hat{\omega}+\frac{3}{16}\hat{\omega}^3+\frac{\hat{\omega}^5}{32}\right), \tag{B.11}$$

$$e_{10} \approx i\frac{1}{2}\left\{\frac{1}{8}\sqrt{\pi}\mathrm{e}^{-\hat{\omega}^2/4}\left(\frac{3}{\hat{\omega}^2}+\frac{3}{2}+\frac{3}{8}\hat{\omega}^2+\frac{\hat{\omega}^4}{16}\right)\right\}, \tag{B.12}$$

$$e_{11} \approx i\sqrt{\pi}\mathrm{e}^{-\hat{\omega}^2/4}\left(\frac{1}{\hat{\omega}}+\frac{\hat{\omega}}{2}+\frac{\hat{\omega}^3}{8}\right). \tag{B.13}$$

[1] P.H. Diamond, S.-I. Itoh, K. Itoh and T.S. Hahm, Plasma Phys. Control. Fusion **47**, R35 (2005).
[2] K. Itoh, S.-I. Itoh and A. Fukuyama, *Transport and Structual Formation in Plasma* (IOP, 1999, Bristol).
[3] A. Yosizawa, S.-I. Itoh and K. Itoh, *Plasma and Fluids Turbulence* (IOP, 2002, Bristol).
[4] K. Itoh and S.-I. Itoh, J. Plasma Fusion Res. **81**, 972 (2005).
[5] K. Hallatschek, Phys. Rev. Lett. **93**, 065001 (2004).

[6] N. Winsor, J.L. Johnson and J.J. Dawson, Phys. Fluids. **11**, 2248 (1968).
[7] V.B. Lebedev, P.N. Yushmanov, P.H. Diamond, S.V. Novakovskii and A.I. Smolyakov, Phys. Plasmas **3**, 3023 (1996).
[8] S.V. Novakovskii, C.S. Liu, R.Z. Sagdeev and M.N. Rosenbluth, Phys. Plasmas **4**, 4272 (1997).
[9] F.L. Hinton and M.N. Rosenbluth, Plasma Phys. Control. Fusion **41**, A653 (1999).
[10] H. Sugama and T.-H. Watanabe, Phys. Plasmas **13**, 012501 (2006).
[11] H. Sugama and T.-H. Watanabe, J. Plasma Phys. **72**, 825 (2006).
[12] T. Watari, Y. Hamada, A. Fujisawa, K. Toi and K. Itoh, Phys. Plasmas **12**, 062304 (2005).
[13] S. Satake, K. Okamoto, N. Nakajima, H. Sugama, M. Yokoyama and C.D. Beidler, Nucl. Fusion **45**, 1362 (2005).
[14] T.S. Halm, Plasma Phys. Control. Fusion **42**, A205 (2000).
[15] K. Hallatschek, Phys. Rev. Lett. **84**, 5145 (2000).
[16] K. Hallatschek, Phys. Rev. Lett. **86**, 1223 (2001).
[17] K. Itoh, K. Hallatshek and S.-I. Itoh, Plasma Phys. Control. Fusion **47**, 451 (2005).
[18] A. Fujisawa, K. Itoh, H. Iguchi, K. Matsuoka, S. Okamura, A. Shimizu, T. Minami, Y. Yoshimura, K. Nagaoka, C. Takahashi, M. Kojima, H. Nakano, S. Ohsima, S. Nishimura, M. Isobe, C. Suzuki, T. Akiyama, K. Ida, K. Toi, S.-I. Itoh and P.H. Diamond, Phys. Rev. Lett. **93**, 165002 (2004).
[19] Y. Nagashima, K. Hoshino, A. Ejiri, K. Shinohara, Y. Takase, K. Tsuzuki, K. Uehara, K. Kawashima, H. Ogawa, T. Ida, Y. Kusama and Y. Miura, Phys. Rev. Lett. **95**, 095002 (2005).
[20] G.D. Conway, B.S. Scott, J. Shirner, M. Reich, A. Kendi and the ASDEX Upgrade Team, Plasma Phys. Control. Fusion **47**, 1165 (2005).
[21] T. Ido, Y. Miura, K. Kamia, Y. Hamada, H. Hoshino, A. Fujisawa, K. Itoh, S.-I. Itoh, A. Nishizawa, H. Ogawa, Y. Kusama and JFT-2M group, Plasma Phys. Control. Fusion **48**, S41 (2006).
[22] E.A. Frieman and Liu. Chen, Phys. Fluids **25**, 502 (1982).
[23] R.D. Hazeltine and J.D. Meiss, *Plasma Confinement* (Addison-Wesley, Redwood City, California, 1992) p.125, p.325.